NWRA NorthWest Research Associates - www.nwra.com

NWRA-BeCR-05-R303 30 November 2005

Laboratory and Numerical Experiments Supporting the Improvement of Vortex Predictions in the Fastwake Numerical Code and Studies of Velocity Decay in Stratified Turbulence

Final Report for Tasks 1 and 3 for
ONR Contract N00014-99-C-0169

By

Donald P. Delisi, Robert E. Robins, and Marie-Pascale Lelong

DISTRIBUTION STATEMENT A
Approved for Public Release
Distribution Unlimited

For

Dr. Ronald Joslin
Office of Naval Research
Ballston Tower One
800 N. Quincy Street
Arlington, VA 22217

1. Introduction

This report documents the results of ONR Contract N00014-99-C-0169. Three tasks were performed on this contract. The first task was to determine, through laboratory experiments and numerical simulations, how a vortex pair detrains fluid as a function of time. The motivation for this study was to determine how the fluid in a migrating vortex cell changes as the vortex pair migrates through the fluid. This study was performed in order to allow SAIC to compare predictions from the FASTWAKE code to experimental measurements. In the experimental part of the study, a vortex pair was generated by a lifting wing, and the detrainment of fluid from the vortex cell was determined for different values of Froude number. These results were then simulated with a 3-D numerical code. The results from this task are presented in Section 2.

The second task in this contract was to determine the existence of oceanographic data that might be useful in understanding the results of a previous study. The results of this task are presented in a separate document (Lai and Delisi, 2005).

The third task in this contract was to numerically model the turbulent flow behind a grid. The motivation for this study was to compare the flow behind a grid from experimental measurements to predictions from numerical simulations, in order to determine whether the numerical model could be useful in elucidating the physics in experimental measurements that were obtained far downstream of the grid. The results from this task, as well as corresponding measurements from a complementary laboratory experiment, are presented in Section 3.

2. Laboratory and Numerical Studies of Detrainment from a Vortex Cell

In order to correctly model the evolution of a vortex pair in a stratified fluid, it is necessary to simulate accurately the detrainment of fluid from the vortex cell. The reason for understanding this detrainment is that the buoyancy of the vortex cell as a function of time is dependent on the density of the fluid in the cell relative to the density of the fluid outside the cell. If the density of the fluid in the cell is the same as that outside the cell, there will be no net buoyancy on the cell. If, on the other hand, the density of the fluid in the cell is different than the density of the fluid outside the cell, there will be a net buoyancy on the cell. In this case, the vertical migration of the cell will be different than if there were no net buoyancy. Thus, to model the vertical migration of the cell correctly, the net buoyancy in the cell must be determined. Since the cell initially contains the density of the fluid at the generating depth of the vortex pair, we must determine how the fluid in the vortex cell detrains from the cell with time and vertical distance.

In the laboratory part of this study, we used wings in our towing tank to generate the vortex pairs. As a lifting wing is towed down the tank, the wing generates a vortex pair that migrates downward, toward the floor of the tank. The experiments were performed in the NorthWest Research Associates (NWRA) towing tank. This towing tank measures 10 m long, 1 m wide, and 1 m deep. The wing was a curved, flat plate,

and had a span of 2 inches and a chord of 1 inch (Figure 1). The measured coefficient of lift vs. angle of attack (C_L-α) curve for this wing is shown in Figure 2. For the measurements reported here, the wing was towed down the tank at a speed of 250 cm/s at angles of attack from 4 to 13 degrees.

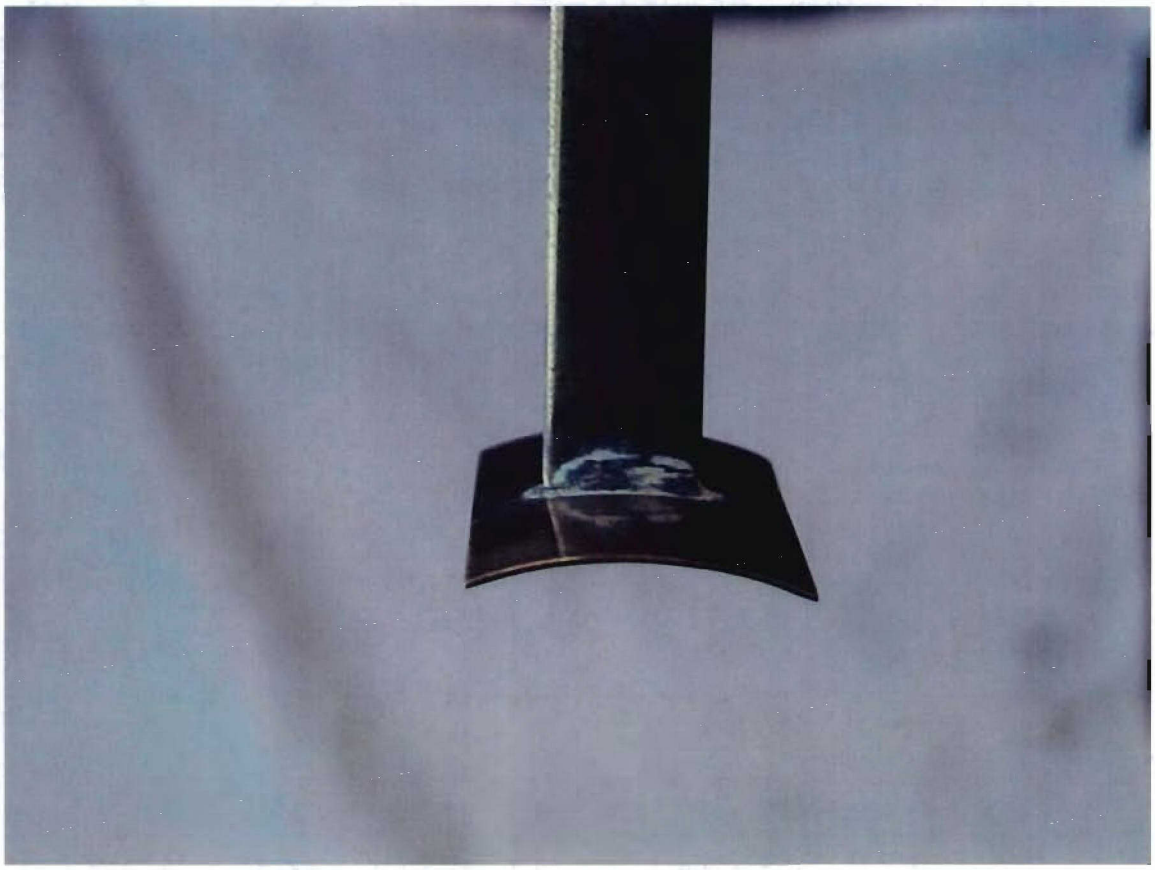

Figure 1. Photograph of the wing used to generate vortices in these experiments.

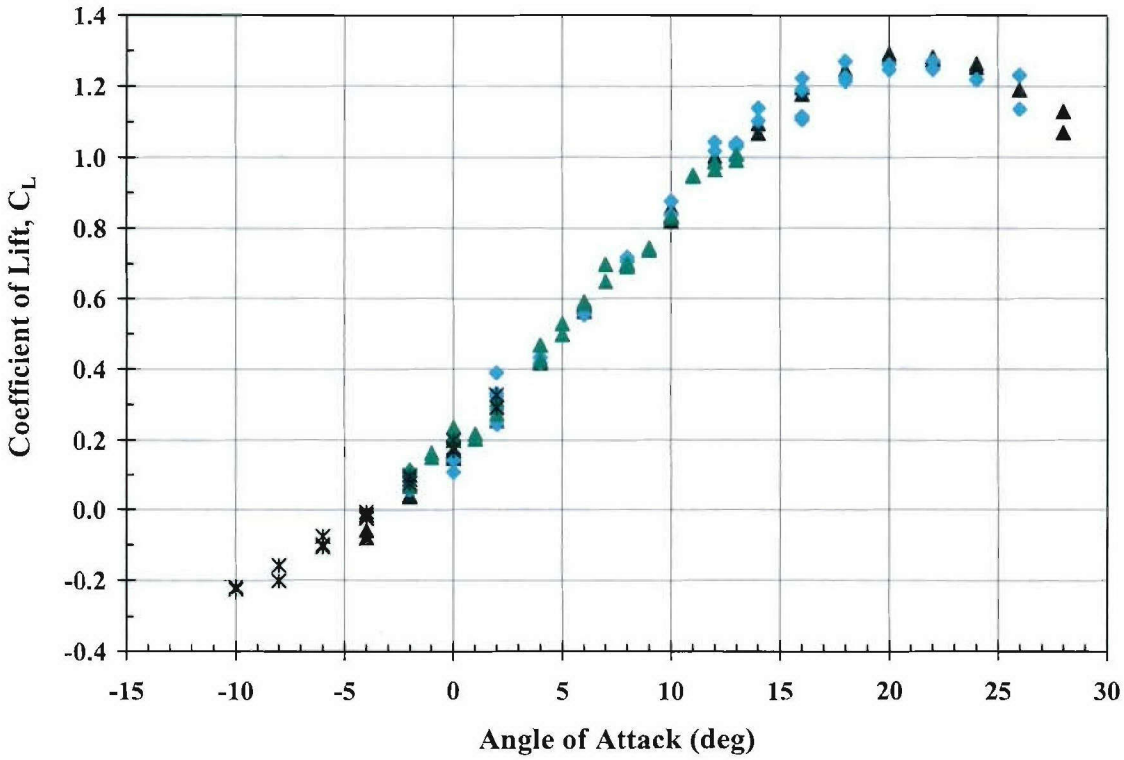

Figure 2. Measured coefficient of lift vs. angle of attack for the wing used in these experiments.

A counter-rotating vortex pair consists of two vortex cores surrounded by turbulent fluid in the vortex cell (Figure 3). Two laboratory studies of detrainment were performed. In the first study, we measured the detrainment of fluid from the entire vortex cell. In the second study, we measured the detrainment of fluid only from the vortex cores. Both of these studies are documented below.

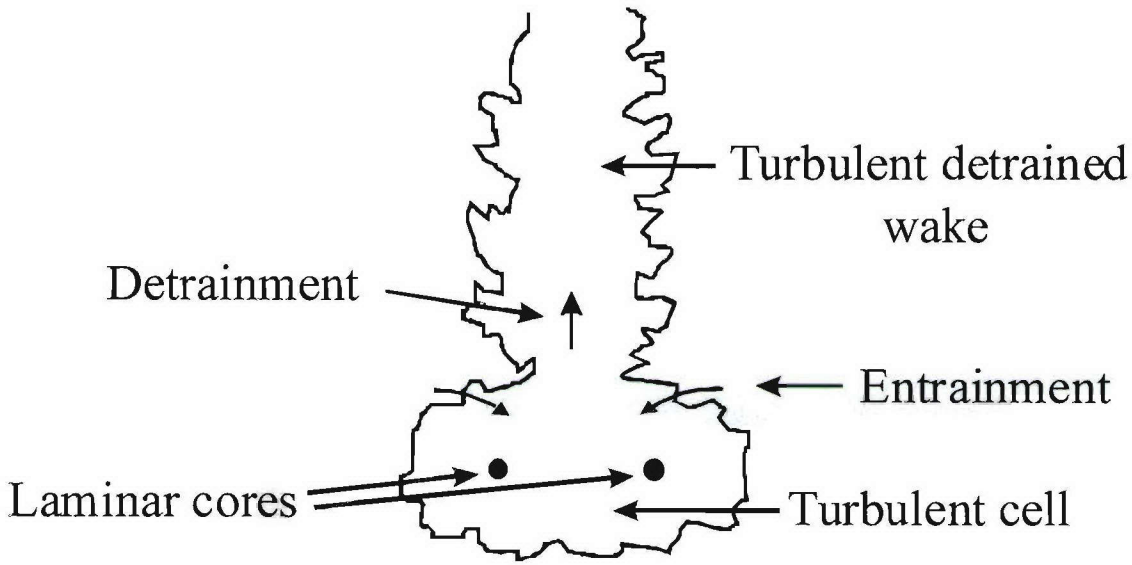

Figure 3. A schematic drawing of our current view of a counter-rotating vortex pair migrating downwards. The two vortex cores are laminar and are surrounded by turbulent fluid in the vortex cell. Fluid is detrained from the cell into a detrained wake. (Note that a laminar vortex cell does not detrain a significant amount of fluid. This is one of the primary differences between a laminar vortex cell and a turbulent cell.)

2.1. Laboratory Studies of Detrainment from a Vortex Cell

For the laboratory studies of detrainment from a vortex cell, we used nearly neutrally buoyant particles to follow the flow. To perform a run, we first injected the particles into the flow field in the test section at the level of the wing. When the wing passed through the test section, the vortices picked up the particles and carried them down into the tank, towards the floor (Figure 4). Figure 5 is the same photograph as in Figure 4, but with the addition of a line that shows the limits of the vertical migration of the particles (the thin, solid line) as well as the depth of vortex linking. The region above the depth of linking shows the two-dimensional (2-D) vortex region. The region below the depth of linking shows the three-dimensional (3-D), or vortex ring, region. The vortices evolve from 2-D line vortices to 3-D vortex rings by the well-known Crow instability (Crow, 1970).

Figure 4. Photograph of the laboratory test section from the side of the tank after the passage of the wing. Nearly neutrally buoyant particles were placed near the top of this photo, in the path of the wing. The vortices, generated by the passage of a lifting wing, picked up the particles and carried them downwards, towards the floor of the tank. This photograph shows the region of two-dimensional flow, in the top half of the tank, where the particles are uniformly distributed, as well as three-dimensional vortex rings, in the bottom half of the tank.

To estimate the detrainment, we start with photographs like Figure 5 and add the depth of the wing (H = 0), and the depth below the wing (see Figure 6). To be able to compare measurements from different wings, we use nondimensional depth, H, where $H = h/b_o$, where h is dimensional depth and b_o is the initial horizontal separation of the vortex pair. We estimated b_o by viewing the initial vortex generation from the wing using a camera located above the tank. From Figure 6, we then add bounding lines around one vortex ring, so we can estimate the detrainment for a unit length of the vortex wake (Figure 7). Note that, in Figure 7, b_o is equal to one unit of H, and one wingspan corresponds to approximately 1.1H. Thus, the wingspan is small relative to the scale of the vortex rings. From Crow (1970), we know that the dominant long wavelength instability is approximately $8.6b_o$. From Figure 7, we estimate that the instability is around $8.4b_o$.

Figure 7 is a blend of Figures 4 and 6, with the addition of two parallel lines bounding one vortex ring and lines at constant values of H. The vertical scale showing the depth in nondimensional units, H, has been retained from Figure 6. The region above H = 1 has been deleted for clarity. We use photographs like Figure 7 for our analysis.

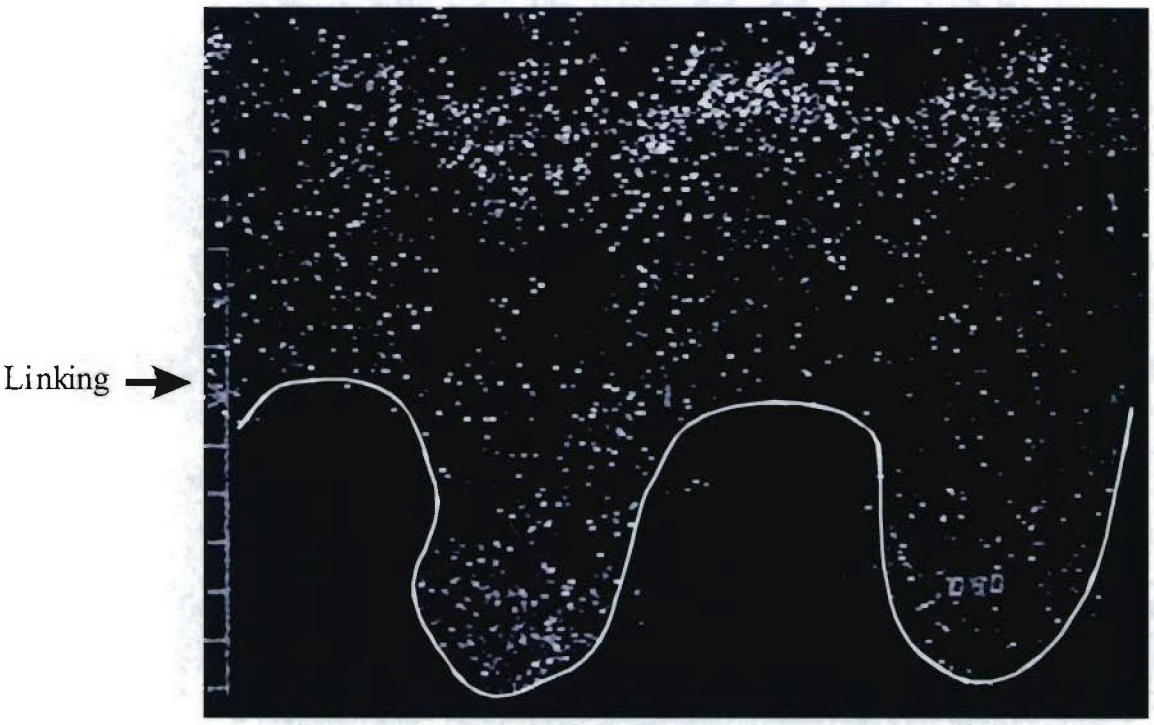

Figure 5. Same as Figure 4, but with the addition of a thin, solid line showing the limits of the vertical migration of the particles and an arrow showing the depth of vortex linking. The wing passed by the test section at the top of this photograph. The region above the depth of linking shows the two-dimensional vortex region. The region below the depth of linking shows the three-dimensional, or vortex ring, region.

The procedure for estimating detrainment is the following:

a. Figure 7 shows parallelograms of unit length in the axial direction (the direction of travel of the wing) and unit values of depth, H. The number of particles in each parallelogram is counted.
b. We sum the number of particles in all the parallelograms. This number is the total number of particles that are carried by the vortices, which is the same as the number of particles initially in the vortex cell. (With the way we seed the initial particles, no (or, at least, very few) particles were below the level H = 1 when the wing passed. Thus, all particles below H = 1 were carried there by the vortices.)
c. We compute the percent of initial particles remaining in the vortex cell at a given depth, H*, as the number of particles below H* divided by the total number of particles initially in the vortex cell.

We use particles for our estimates of detrainment since dye will diffuse and is difficult to measure quantitatively. Particles, on the other hand, remain distinct, and can be counted rather easily.

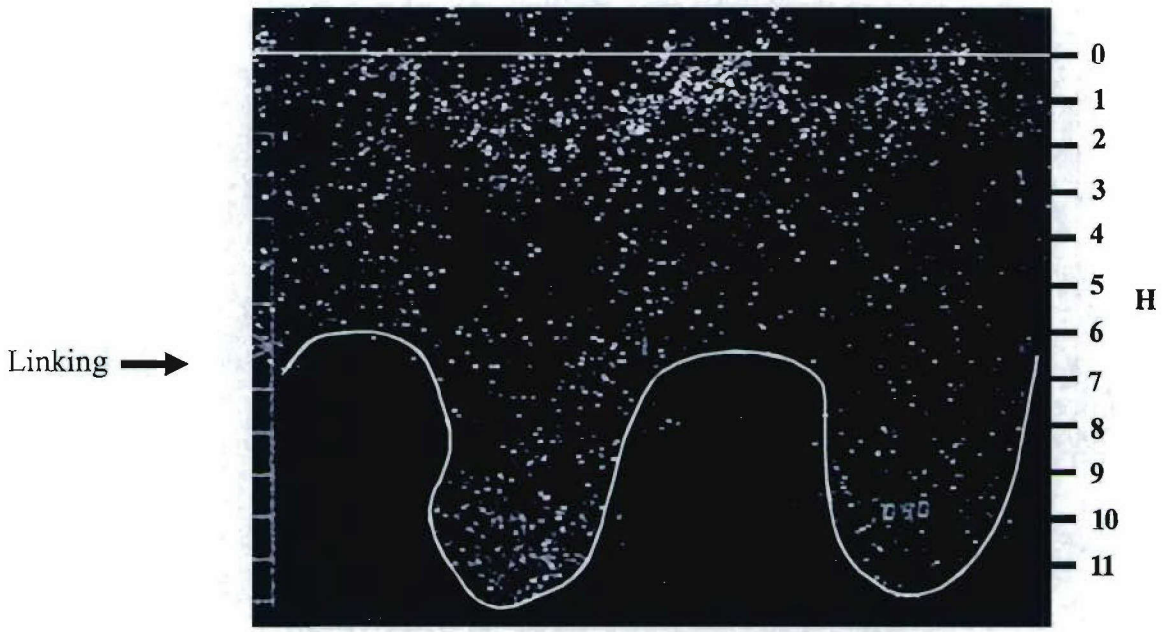

Figure 6. Same as Figure 5, but with the addition of a thin, solid line showing the depth of the wing (at H=0) and a vertical scale showing the depth in nondimensional units, H. Note that one wingspan on this plot corresponds to approximately 1.1H. Thus, the wingspan is small relative to the scale of the vortex rings.

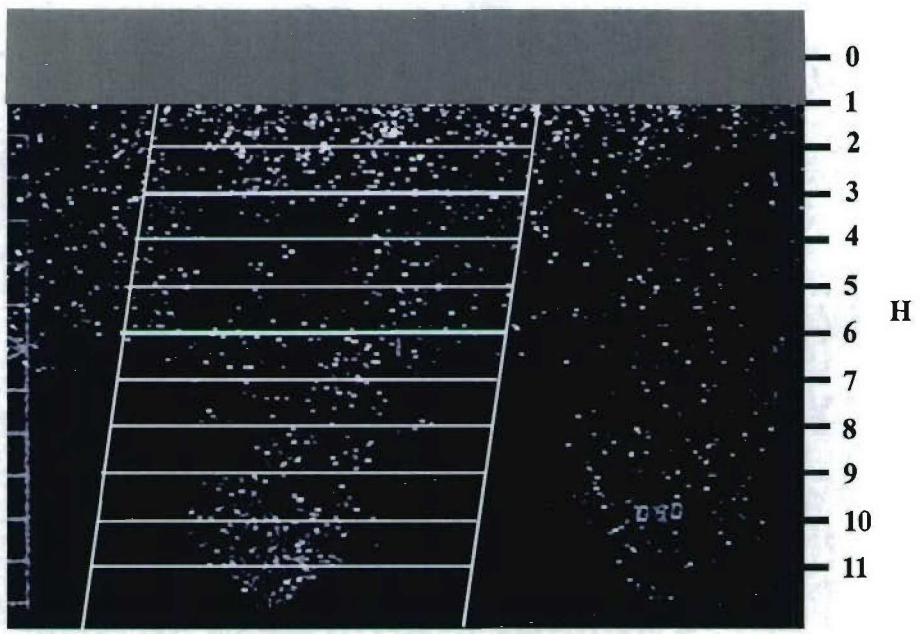

Figure 7. Same as Figure 4, but with the addition of two parallel lines bounding one vortex ring, lines at constant values of H, and a vertical scale showing the depth in nondimensional units, H. The region above H = 1 has been deleted for clarity.

Figure 8 shows the results for detrainment in a nonstratified fluid, with N = 0, where N is the Brunt-Vaisala frequency defined by $N^2 = -(g/\rho)(d\rho/dz)$, where g is gravitational acceleration, ρ is density, and z is the vertical dimension. Measurements are shown for four runs for each of three different wing angles of attack (red = 13 deg, green = 8 deg, and blue = 4 deg). The measurements have been normalized to H = 1.5, the midpoint of the parallelogram spanning from H = 1 to H = 2. For the runs shown in Figure 8, the median number of total particles was 304, yielding around 30 particles in each parallelogram.

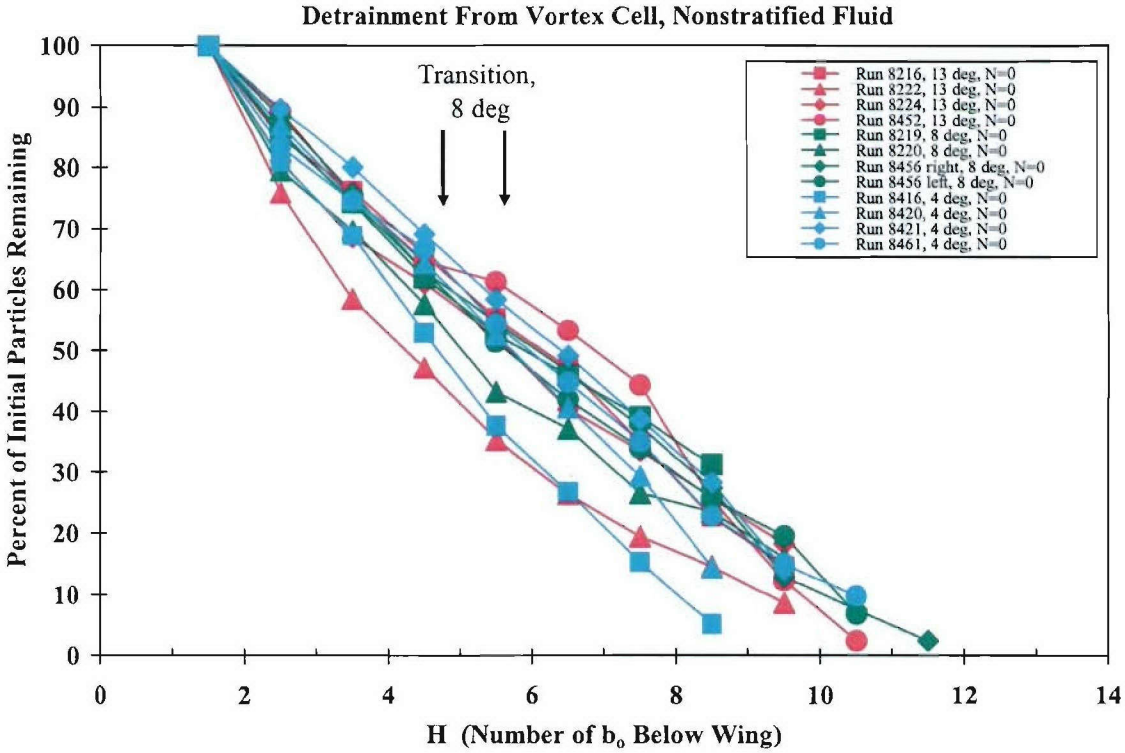

Figure 8. Laboratory measurements of detrainment from the vortex cell in a nonstratified fluid when the entire cell initially contains particles. Four runs are shown for three different wing angles of attack (red = 13 deg, green = 8 deg, blue = 4 deg). The vortices were generated by towing a wing down the tank at a tow speed of 250 cm/s.

In Figure 8, the vortices are 2-D for H = 0 to around H = 4.5 to 5.5. For H greater than 5.5, the vortices are vortex rings. We note that the slopes of the lines in Figure 8 do not change significantly around H = 4.5 to 5.5. Thus, the detrainment rate from vortex rings (H greater than 5.5) is nearly the same as the detrainment rate from 2-D vortex lines (H less than 4.5).

Figure 9 shows the average of the runs shown in Figure 8. The error bars show the standard deviations at several values of H. This figure shows that the detrainment is nearly constant for all three angles of attack.

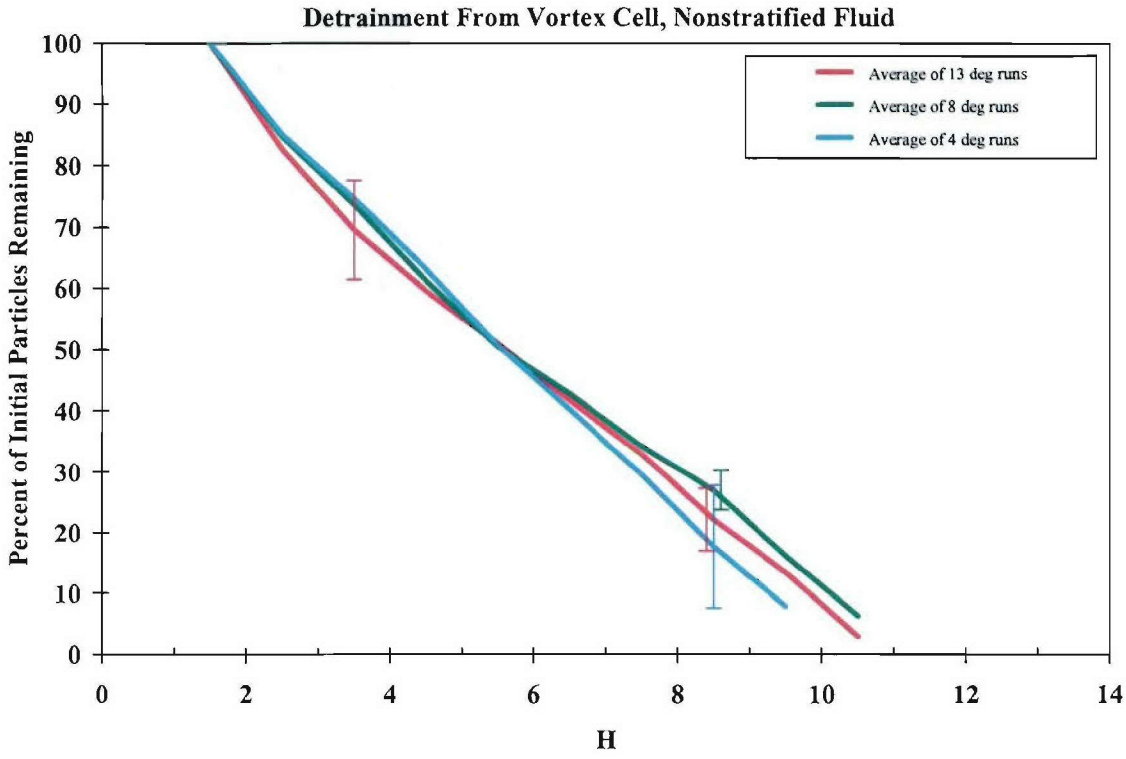

Figure 9. Average of the runs shown in Figure 8. The error bars show the standard deviations at several values of H.

Figure 10 shows the data in Figure 9, with the addition of the black line, which is the average of the red, green, and blue lines in Figure 9. The error bars show the standard deviations of all the data at a given value of H. We use the black line as the average detrainment from a vortex pair in a nonstratified fluid.

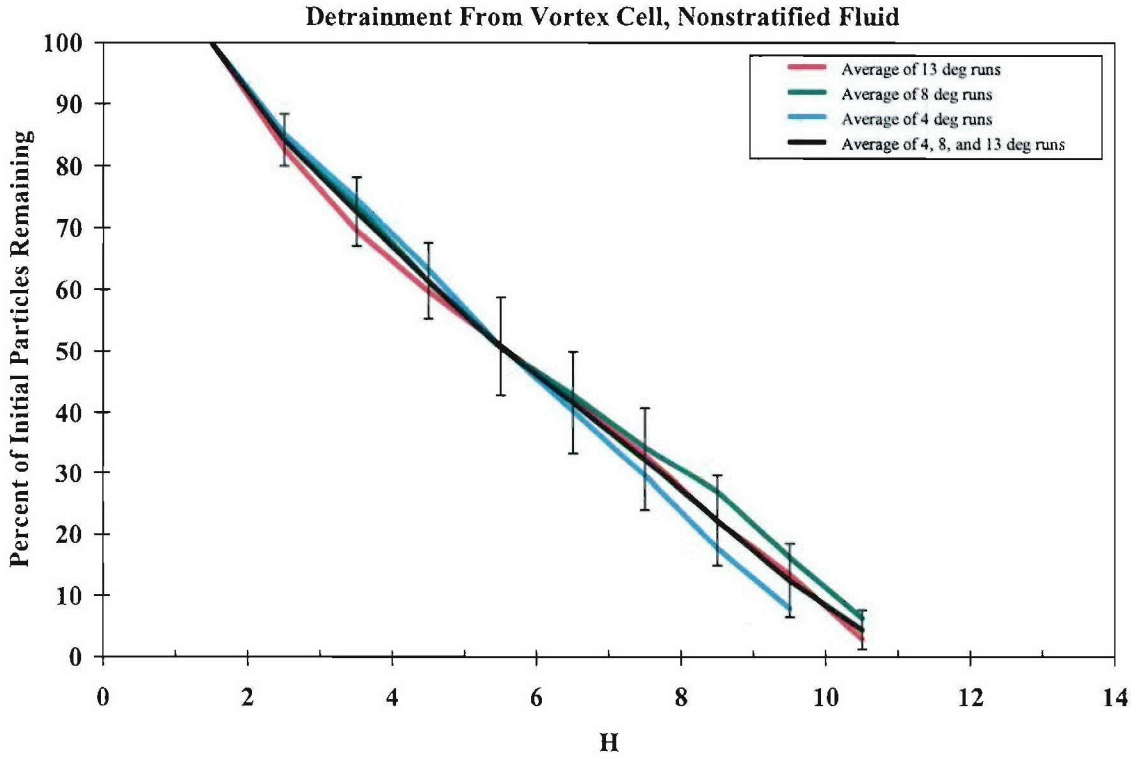

Figure 10. Same as Figure 9, with the addition of the black line which is the average of the red, green, and blue lines. The error bars show the standard deviations of all the data at given values of H.

The measurements in Figures 8 through 10 were repeated for vortex pairs in stratified fluids. These flows are characterized by the Froude number, where the Froude number is defined as $Fr = V_o/Nb_o$, where V_o is the initial vertical velocity of the vortex pair, and N and b_o are defined above. As the stratification increases (N increases), the Froude number decreases. V_o was measured by using dye to visualize the cores of the vortices, and tracking the vertical descent of the vortices with time. For the data shown here, V_o ranged from 5.6 to 11.3 cm/s.

Figure 11 shows the same measurements as Figure 10, with the addition of measurements performed with different values of Froude number. This figure shows that, as the stratification, N, increases, (the Froude number decreases), the rate of detrainment from the vortex cell increases. The black line in this figure (for N = 0, or Froude number of infinity) is the same as the black line in Figure 10.

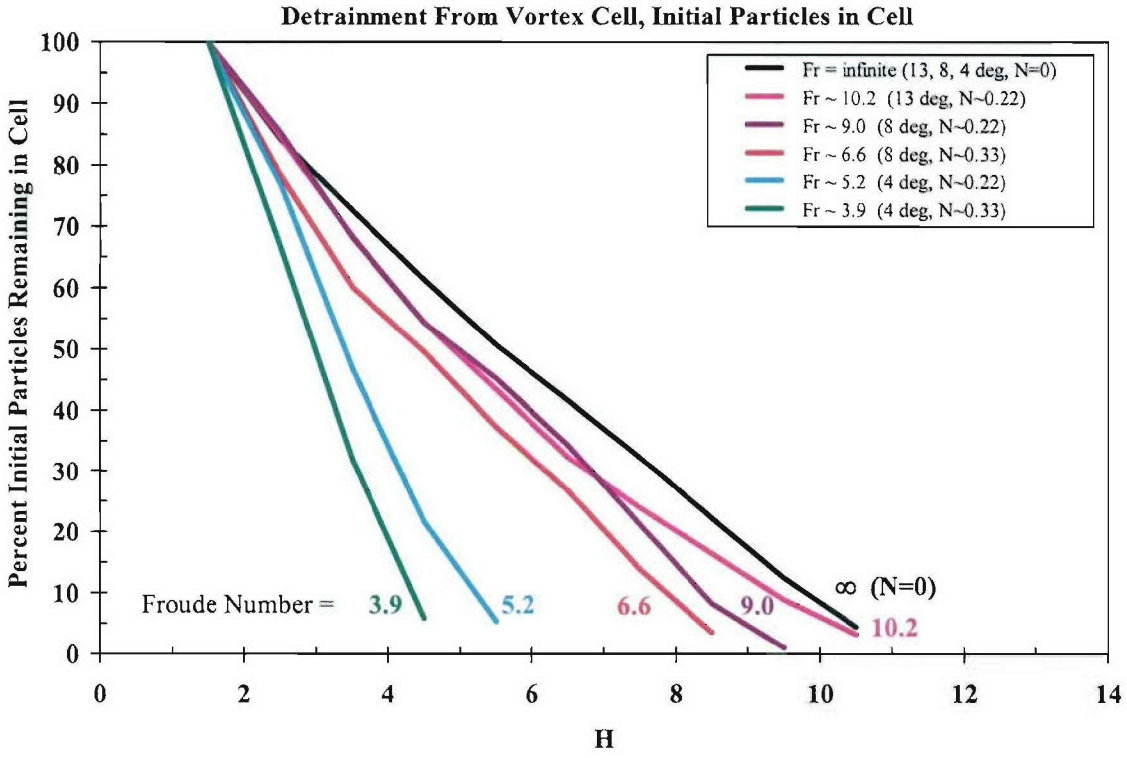

Figure 11. Same as Figure 10, with the addition of laboratory measurements performed with different values of Froude number. As the stratification increases (Froude number decreases), the rate of detrainment from the vortex cell increases. The black line in this figure is the same as the black line in Figure 10.

2.2. Numerical Predictions of Detrainment from a Vortex Cell

In order to compare numerical estimates of detrainment with the laboratory results presented in Section 2.1, we used an LES code to simulate the laboratory experiments. The TASS code, developed by F. Proctor of NASA's Langley Research Center (Proctor, 1987), was chosen for the simulations because it has the capability of maintaining tight vortex cores and allows the inclusion of an equation for the evolution of a passive scalar.

To replicate the laboratory approach of seeding the vortex cell with particles, we initialized a passive scalar field with a value of unity within the vortex cell and zero outside. Simulations were performed for a zero stratification case (infinite Fr) and a high stratification case (Fr =4) to compare with laboratory cases having similar levels of stratification. To replicate the presence of turbulence in the vortex cells in the laboratory cases, we used turbulence fields having initial normalized eddy dissipation rates (ε^*) of 0.5 and 1.0, values which bracketed the turbulence observed in the vortex cells for the laboratory cases.

To determine the amount of detrainment during the evolution of the vortices, the amount of passive scalar found outside the vortex cell was tracked as a function of time. This quantity was subtracted from the total amount of passive scalar initially in the vortex cell, thus yielding the amount remaining in the vortex cell. The results, expressed as a percentage of passive scalar remaining in the vortex cell, are shown in Figure 12 for the cases N=0 and Fr = 4 with $\varepsilon^* = 1.0$. This figure shows that, as for the laboratory results, increasing stratification causes a faster rate of detrainment. The difference between the laboratory and numerical results is possibly due to the non-local nature of the technique (requiring multiple grid points) used by the code to maintain tight cores.

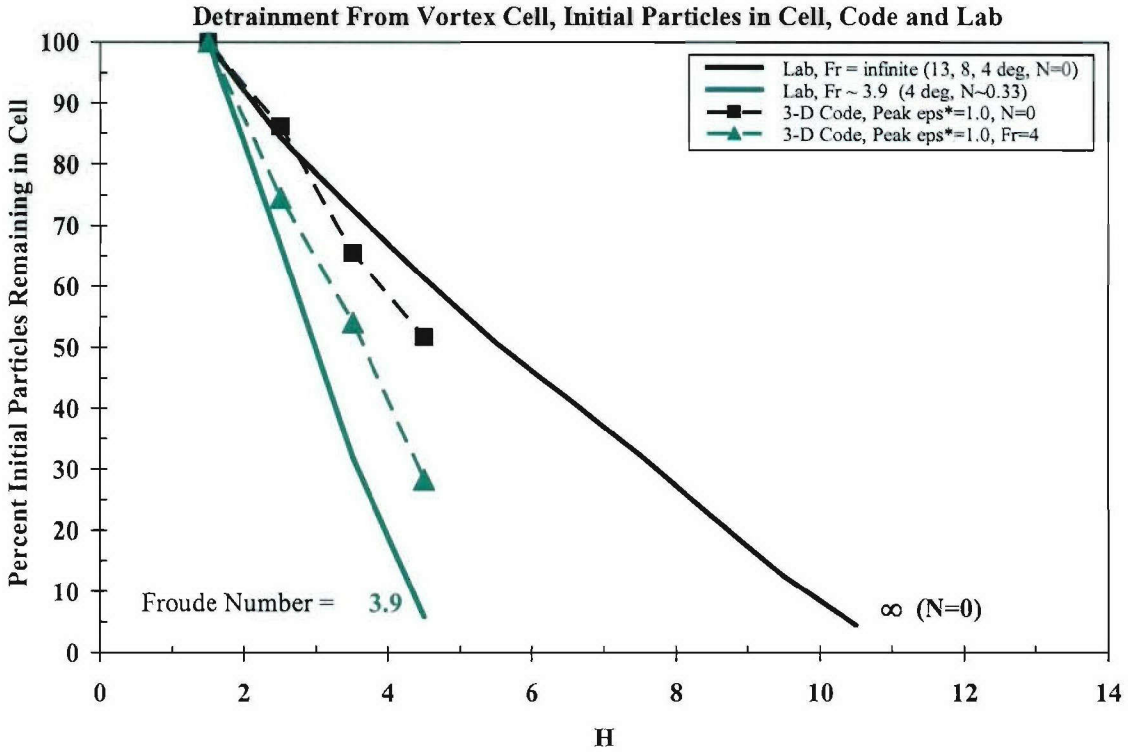

Figure 12. Measurements of detrainment from the vortex cell when the initial particles are distributed throughout the entire cell. Laboratory measurements for Froude number infinity and 3.9, from Figure 11, are shown as the solid lines, and numerical predictions from a 3-D numerical code, for Froude number infinity and 4, are shown as the dashed lines.

2.3. Laboratory Studies of Detrainment from the Vortex Cores

In Section 2.1, we showed the results of laboratory experiments of the detrainment of fluid from the entire vortex cell. In this section, we describe laboratory experiments that measure the detrainment of fluid from only the vortex cores.

To perform these experiments, we use the techniques described in Section 2.1, but we initially place particles in the vortex cores only. To seed particles into the vortex cores, we developed the technique of the "particle cloud" method. Using this method, we place a cloud of particles in the path of the model wing just before the test section. As the wing passes through the cloud of particles, the vortex cores drag the particles in the cores into the test section (Figure 13). Figure 14 shows a photograph of the particles being drawn from the cloud into the vortex cores and into the test section. Figure 15 shows the flow at a later time. Two distinct regions are shown in Figure 15. On the right half of the figure, the particles show a pattern similar to Figure 4. This pattern is the result of particles that were initially distributed throughout the cell. On the left half of Figure 15, we see very few particles, particularly up high in the photo, near depth of the wing. The particles in the lower half of Figure 15 on the left are those that were initially in the vortex cores. Thus, of the particles that were initially in the vortex cores, few are detrained near the depth of the wing, and most of the detrainment occurs during or after vortex linking.

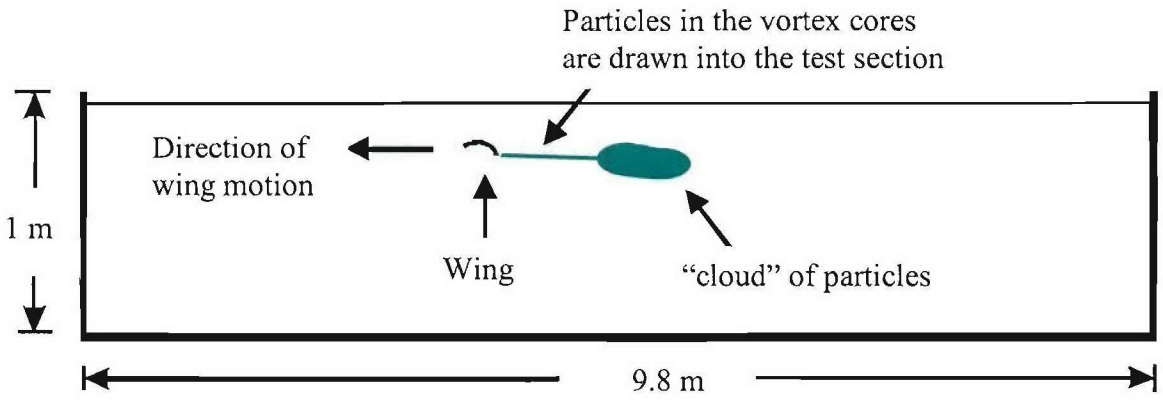

Figure 13. Schematic drawing of the technique for placing neutrally buoyant particles into the laboratory vortex cores.

Figure 14. Photograph from a laboratory experiment of the particle cloud, on the right, with particles in the vortex cores on the left. The wing passed from right to left in the photograph. The photograph shows the paths of particles displayed in the schematic drawing in Figure 13.

Figure 15. Similar to Figure 14, but at a later time. On the right half of the photograph, where the particles were initially distributed throughout the vortex cell, we see an evolution similar to Figure 4. On the left side of the photograph, where the particles were initially only in the vortex cores, there is very little detrainment at depths above the depth of vortex linking.

Results from the analysis of photographs such as Figure 15 are shown in Figure 16. The solid lines in this figure show the results from the initial particles being distributed throughout the vortex cell, and are reproduced from Figure 11. Results for a nonstratified (Froude number = infinity) fluid (black, solid line) and for a Froude number of 6.6 (red, solid line) are shown. The dashed lines in Figure 16 show the detrainment when only the vortex cores contain the initial particles. Results for a nonstratified (Froude number = infinity) fluid (black, dashed line) and for a Froude number of 7.1 (red, dashed line) are shown. The dashed lines in Figure 16 show that, when only the cores are seeded, there is little detrainment until the time of vortex linking, around H ~ 4.5 to 5.5. Thus, Figure 16 shows that the detrainment from the vortex cores is dramatically different than the detrainment from the vortex cell. Note that over 90% of the particles initially in the vortex cores remain in the cores until H is greater than about 4.5. At this depth, when the particles were initially distributed throughout the entire cell, nearly half of the particles were detrained from the cell. Thus, there is relatively little detrainment from the vortex cores relative to the detrainment from the vortex cell.

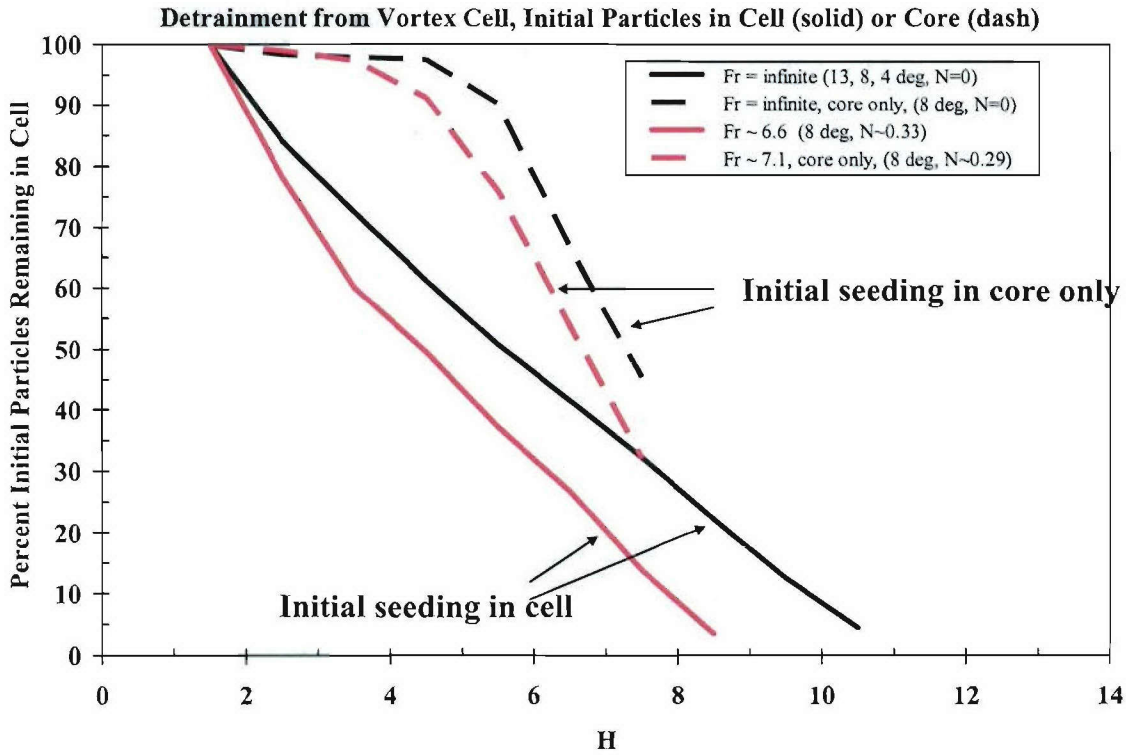

Figure 16. Laboratory measurements of detrainment from the vortex cores (dashed lines) and detrainment from the vortex cell (solid lines from Figure 11). When only the cores are seeded, there is little detrainment until the time of vortex linking. Note that over 90% of the particles initially in the vortex cores remain in the cores until H is greater than about 4.5. At this depth, nearly half of the particles in the vortex cells were detrained from the cell. These results are consistent with the photographs in Figures 4 and 15.

2.4. Summary of Studies of Detrainment from the Vortex Cores

The above results show that detrainment from the vortex cell is dramatically different than the detrainment from the vortex cores. For detrainment from the vortex cell:

- For no ambient stratification, little or no ambient turbulence, and no ambient shear, about half (50%) of the particles initially in the vortex cell are detrained by H ~ 5.5 (Figure 11).
- With increasing stratification (decreasing Froude number), there is a faster rate of detrainment from the vortex cell, both in the laboratory (Figure 11) and in numerical simulations (Figure 12).

For detrainment from the vortex cores only:

- When only the cores are seeded, there is little detrainment until the time of vortex linking (Figure 16).
- With increasing stratification (decreasing Froude number), there is a faster rate of detrainment from the vortex cores, but there is still significantly less detrainment from the cores than from the entire cell (Figure 16).

3. Numerical Simulations of the Turbulent Flow Behind a Grid and Supporting Laboratory Experiments

The objective of this task was to numerically model the turbulent flow behind a grid. We have chosen to simulate the turbulence behind a grid in a uniform flow, since this flow can also be generated easily in the laboratory. By comparing the laboratory measurements to the numerical predictions, we hoped to validate the numerical code. The code could then be used to perform simulations that are either difficult or impossible to perform in the laboratory.

3.1 The Near-Field Numerical Model

We first numerically simulated the flow field just behind the grid, in what we call the near-field region of the flow. For these simulations, we resolved the details of turbulence generation by incorporating the grid mesh into the simulations and explicitly computing the flow through the mesh and the generation and shedding of vorticity from the solid surfaces. For these simulations, we use a numerical model (S-FIT) that was designed to simulate density-stratified flows interacting strongly with topography. The numerical code itself has been extensively tested and validated against analytical solutions and laboratory experiments (Winters et al., 2000; Winters and Seim, 2000; Finnigan et al., 2001). This code was ported and compiled on a Cray T3E computer.

The design details for our near-field numerical simulation runs are described below and shown schematically in Figure 17. Our basic approach is to directly simulate flow through a rectangular-barred grid mesh with bar and spacing dimensions close to those used in the laboratory experiments. Due to computational constraints, we could not

simulate the entire cross sectional area of the laboratory channel. Rather, we simulated the flow through the central section, well away from the channel sidewalls. Our simulation included two horizontal and two vertical bars, as shown in Figure 17.

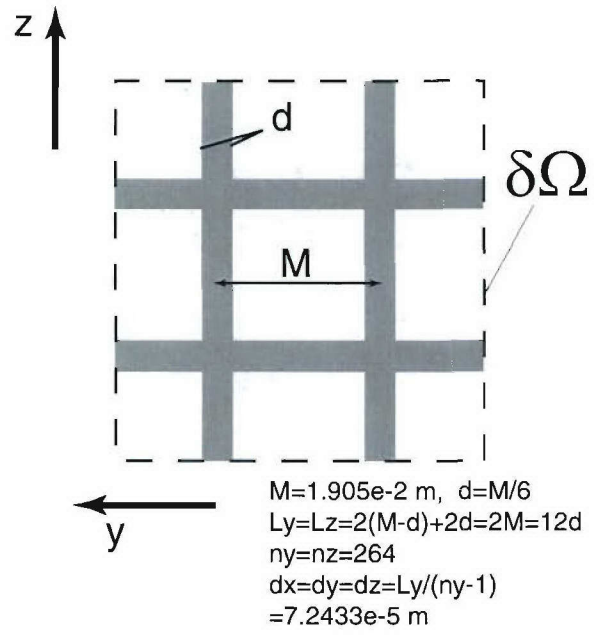

Bar faces are located at grid points (55,77) and (187,209) wit h dy=d/22
δΩ: free-slip computational boundaries.

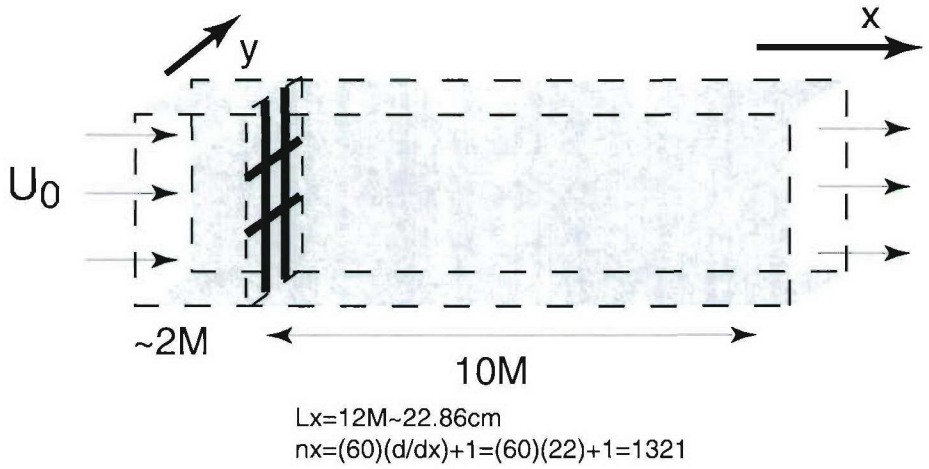

Figure 17. Schematic drawing of the numerical simulations. Two horizontal and two vertical rods were used to simulate the grid flow. The flow passed through the grid from left to right. The total length of the numerical domain was 12M.

Our initial simulation was performed in an unstratified and unsheared flow. To initially begin the computation, an unstratified free-stream flow was accelerated from rest to a speed of 25 cm/s. Model grid-generated turbulent velocities in the box shown in Figure 17 were computed at a spatial resolution of 0.02 cm. For comparison with laboratory measurements, time series of model turbulent velocities at various points on the vertical plane at the end of the computational box were generated. This vertical plane was at a down-stream distance of 8.6M from the grid, where M = 2.076 cm is the linear dimension of the grid mesh.

Figure 18 shows examples of the turbulent velocity time series from the numerical model. The top panel shows the along-stream velocity, u, and the bottom panel shows the cross-stream and vertical velocities, v and w, respectively. The mean u is about 25 cm/s. The mean of the v and w components are zero, as expected for cross-stream flows. While the fluctuating v and w components have similar amplitudes, they are weaker than the fluctuating u component, suggesting that this model turbulence is anisotropic. The anisotropic nature of this model grid-generated turbulence is qualitatively consistent with other laboratory measurements (Liu, 1995).

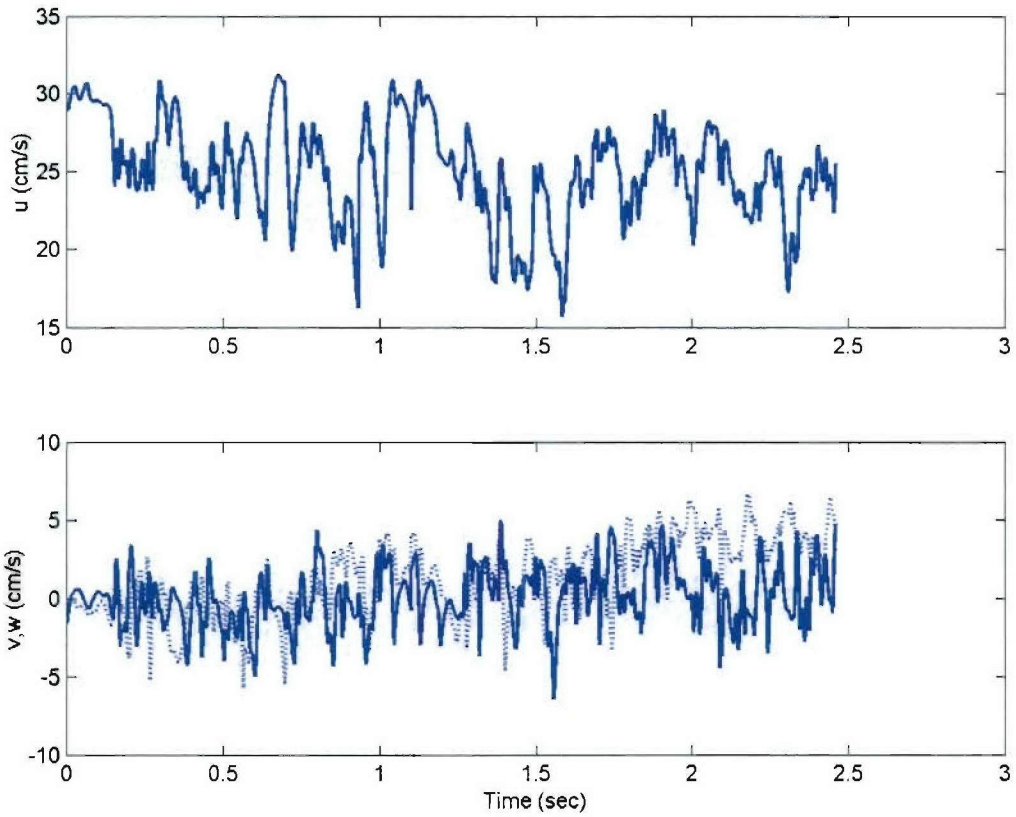

Figure 18. Time series of grid-generated turbulent velocity from the numerical model at 8.6M downstream from grid: top panel – u, bottom panel - v (solid line) and w (dotted line).

Figure 19 shows the u, v, and w wavenumber spectra of the model turbulent velocities, averaged over frequency spectra computed from 16 time series at various y and z locations 8.6M downstream of the grid. The averaging reduces the errors in the spectral estimates. The frequency spectra were converted to wavenumber spectra assuming the frozen field hypothesis.

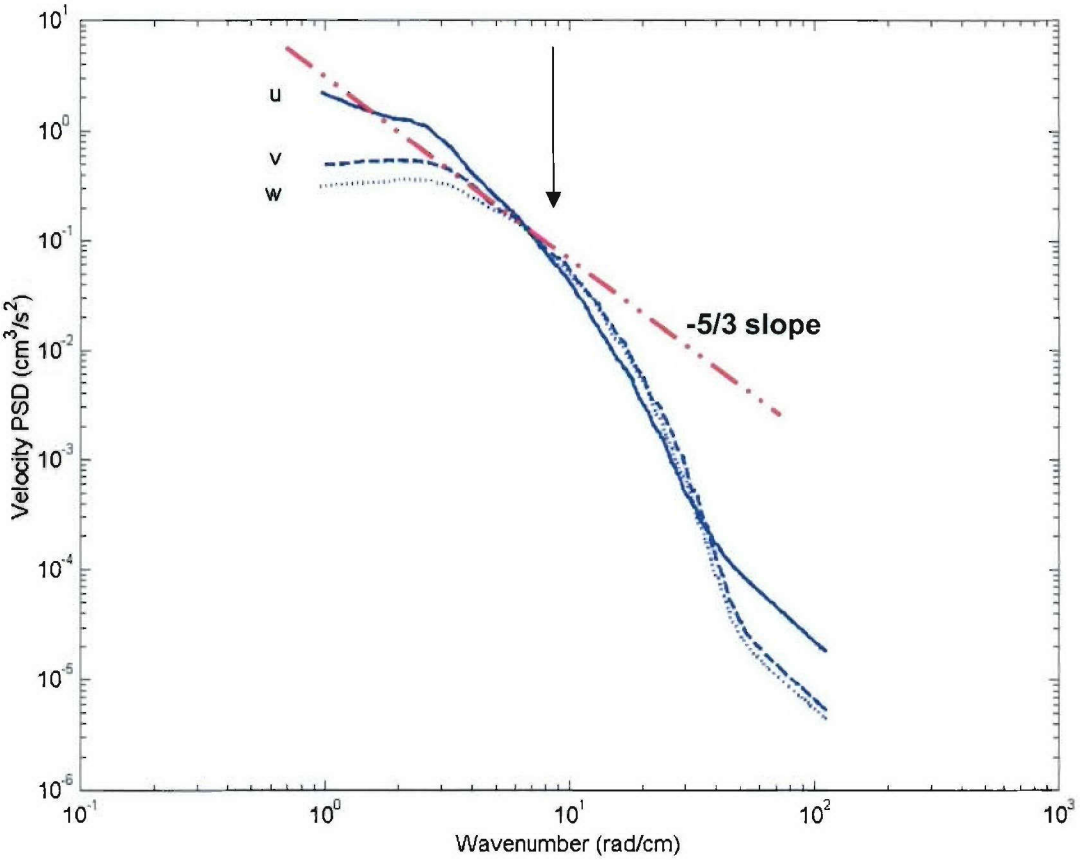

Figure 19. Spectra from the numerical model simulations of u (solid), v (dashed), and w (dotted) velocities at 8.6M downstream from the grid. The observed viscous roll-off is marked by an arrow. The dash-dot straight line indicates a –5/3 slope.

At high wavenumbers between 5 and 40 cm^{-1}, all three components have similar spectral values. At low wavenumbers (below 5 cm^{-1}), the u spectrum is higher than the v and w spectra. This low-wavenumber difference between the u and the v and w components for grid-generated turbulence is qualitatively consistent with observations in the laboratory (Liu, 1995).

The v and w spectra exhibit a –5/3 slope in the inertial subrange. We least-squares fit the v and w spectra to a spectral model of

$$E(k) = 0.55\,\varepsilon^{2/3}\,k^{-5/3}, \qquad (1)$$

where E(k) is spectral power at wavenumber k and ε is dissipation rate, to obtain a dissipation rate, ε, of 8 cm^2s^{-3}. At this dissipation rate, the theoretical viscous roll-off wavenumber is about 9 cm^{-1}. A line with a –5/3 slope is drawn in Figure 19 to illustrate the slope and the roll-off of the spectra. The roll-off wavenumber in the observed v and w spectra is about 8 cm^{-1}, similar to the value expected from theory. The observed roll-off is marked by an arrow in Figure 19.

The energetic features centered at 3 cm^{-1} moved the model u spectrum away from a –5/3 slope. These energetic features are unexpected. We hypothesize that the grid-generated turbulence at this downstream distance (8.6M) is not fully developed. We hypothesize that, further downstream, portions of the energy from these eddies will cascade into smaller scales, erasing the "bump" and resulting in a slope closer to the expected value of –5/3.

3.2. Laboratory Experiments of Flow Behind a Grid

The laboratory experiments of flow behind a grid were performed in a tilt tank in the laboratory, shown schematically in Figure 20. The tank has imensions of 10 m (length) by 45 cm (width) and 30 cm (height), supported by a pivot in the middle. After the tank is filled with stratified water, it is tilted around the pivot for a specific period of time and then leveled. When tilted, a flow is generated in the tank as gravity acts on the density difference in the fluid. The direction of the flow is illustrated by the shaded arrows in the figure. This flow lasts for several seconds after leveling the tank, until surges generated at the ends of the tank propagate into the test section. A grid is installed in the middle of the tank. As water flows past the grid, turbulence is generated behind it. Velocities of the grid-generated turbulence were measured by hot-film probes in the top fluid, 5 cm below the top of the tank. One-component hot film probes were used to measure the along-stream (u) component of the turbulent velocity.

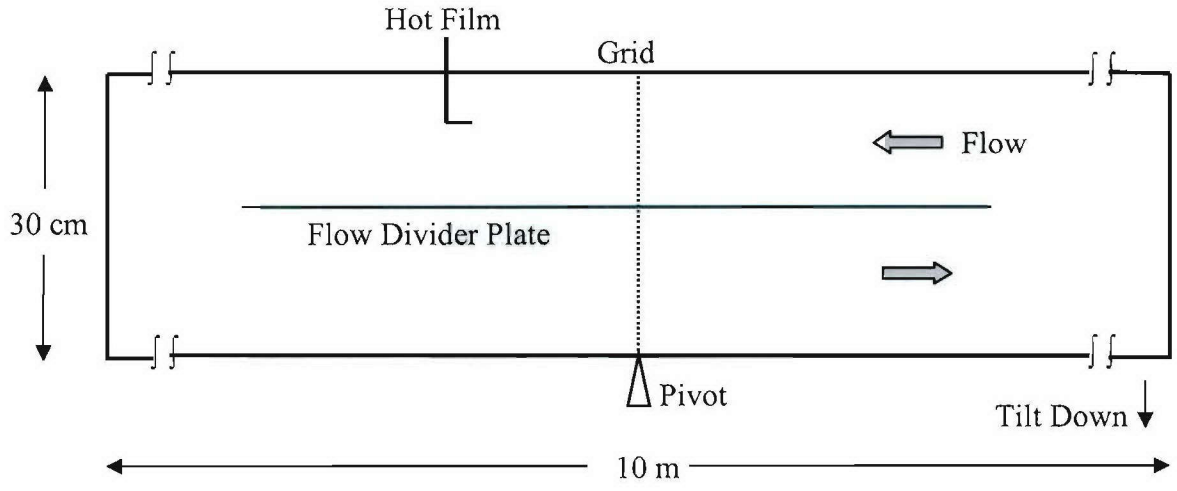

Figure 20. Schematic diagram of the NWRA laboratory tilt tank.

Experiments were performed under two different stratification conditions. In both cases, a mean flow of 20-25 cm/s was generated at the level of the probes. In the first case, turbulence was generated in a homogeneous (nonstratified) fluid. This experiment was performed by filling the tank with a two-layer fluid: a homogeneous lighter fluid in the top half of the tank and a homogeneous denser fluid in the bottom half. After tilting and leveling of the tank, turbulent velocities in the homogeneous top layer were measured.

In the second case, turbulence was generated in a stratified, sheared fluid. This experiment was performed by filling the tank with a linearly stratified fluid with a buoyancy frequency of 1 s^{-1}. After tilting and leveling, a linearly stratified and linearly sheared flow was generated. The Richardson number of the resulting flow was near 0.5. In the near-field of 10M downstream of the grid, stratification and shear are not expected to have a significant influence on the grid-generated turbulence.

Figure 21 shows time series of u velocity measurements from the nonstratified and stratified laboratory experiments, obtained at a distance of $10M_L$ downstream of the grid. These two time series have similar magnitudes. Note that the grid size in the laboratory (M_L=1.9 cm) is slightly different than the grid size (M=2.076 cm) used in the numerical model.

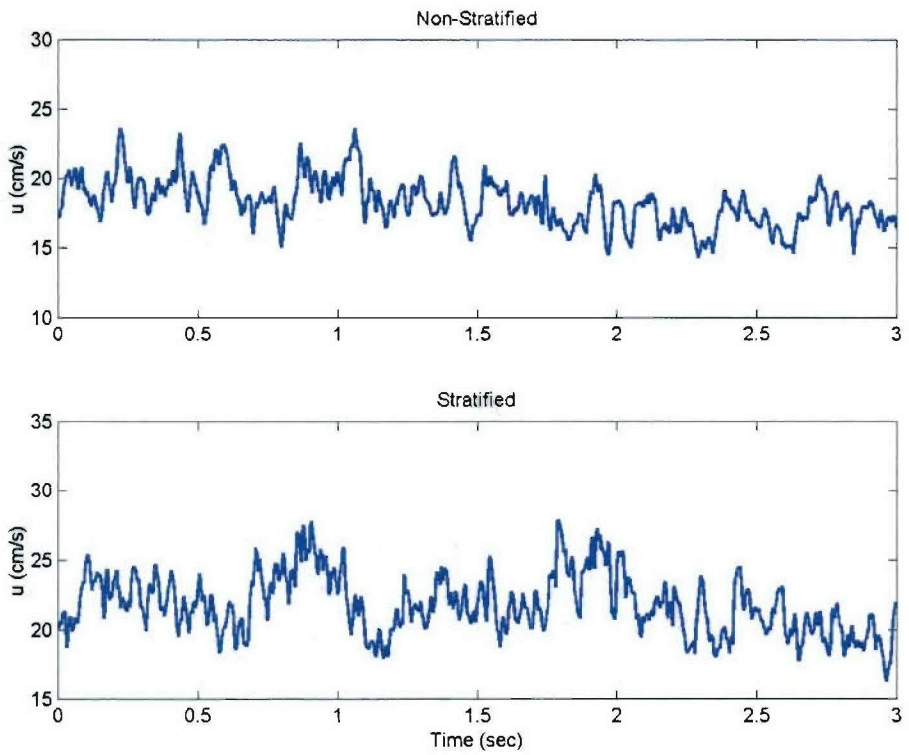

Figure 21. Time series of the u component of grid-generated turbulent velocity from laboratory experiments: nonstratified (top panel) and stratified (bottom panel) flow.

Figure 22 shows the u spectra from the nonstratified (dotted line) and stratified (solid line) laboratory experiments. Both spectra show similar energy levels and a –5/3 slope. The dissipation rates, obtained by performing a least-squares fit of the spectra to the model in Eqn. 1, are 8 and 7 cm^2s^{-3} for the stratified and nonstratified fluid, respectively. These values are similar to the value of 8 cm^2s^{-3} obtained from the numerical model simulation.

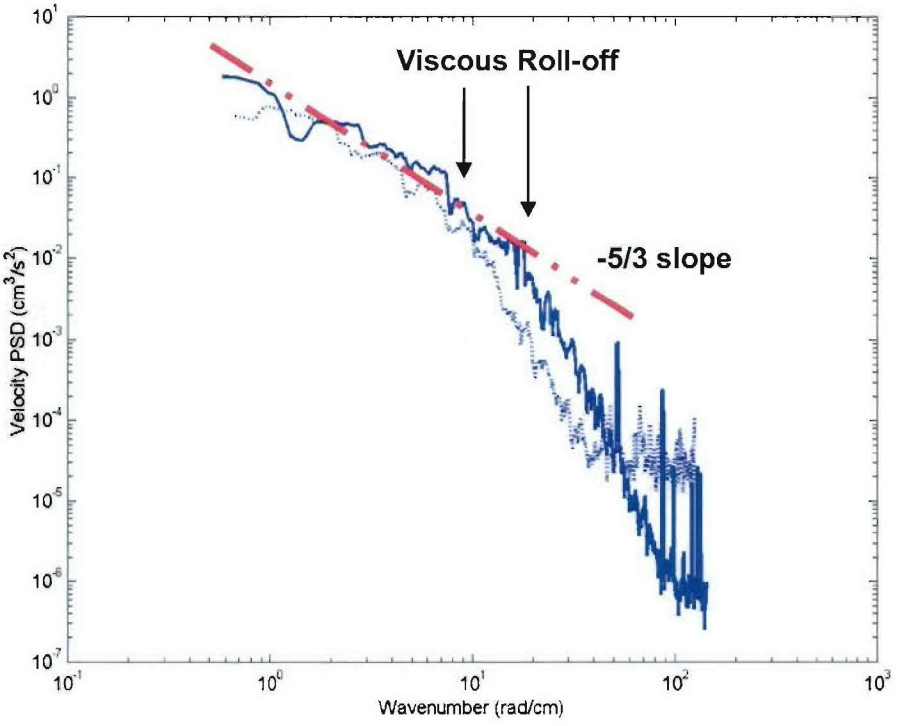

Figure 22. Laboratory measurements of the u spectra of grid-generated turbulent velocity at a downstream distance of $10M_L$, where M_L is the grid size in the laboratory. The solid line represents data for a stratified fluid, and the dotted line for a nonstratified fluid.

While the energy levels of the stratified and nonstratified spectra are similar in Figure 22, the observed viscous roll-off wavenumbers differ by a factor of more than two (20 cm^{-1} for the stratified flow versus 9 cm^{-1} for the nonstratified flow). A roll-off wavenumber of 9 cm^{-1} is expected from the theory of nonstratified turbulent flow. It is possible that the 20 cm^{-1} is related to the stratified and sheared nature of the turbulent flow.

3.3. Laboratory and Model Data Comparison

Figure 23 compares the laboratory observed u spectra (nonstratified and stratified) with the numerical model u spectrum (nonstratified). A –5/3 slope is drawn in the figure

for reference. All three spectra have similar values, to within a factor of two. The energetic "bump" at 3 cm^{-1} for the model data causes the spectrum to deviate from the –5/3 slope. Again, it is hypothesized that the "bump" is the result of not fully developed turbulent eddies. If the turbulence were fully developed, we believe portions of this energy would have cascaded to higher wavenumbers, making the spectral slope closer to –5/3.

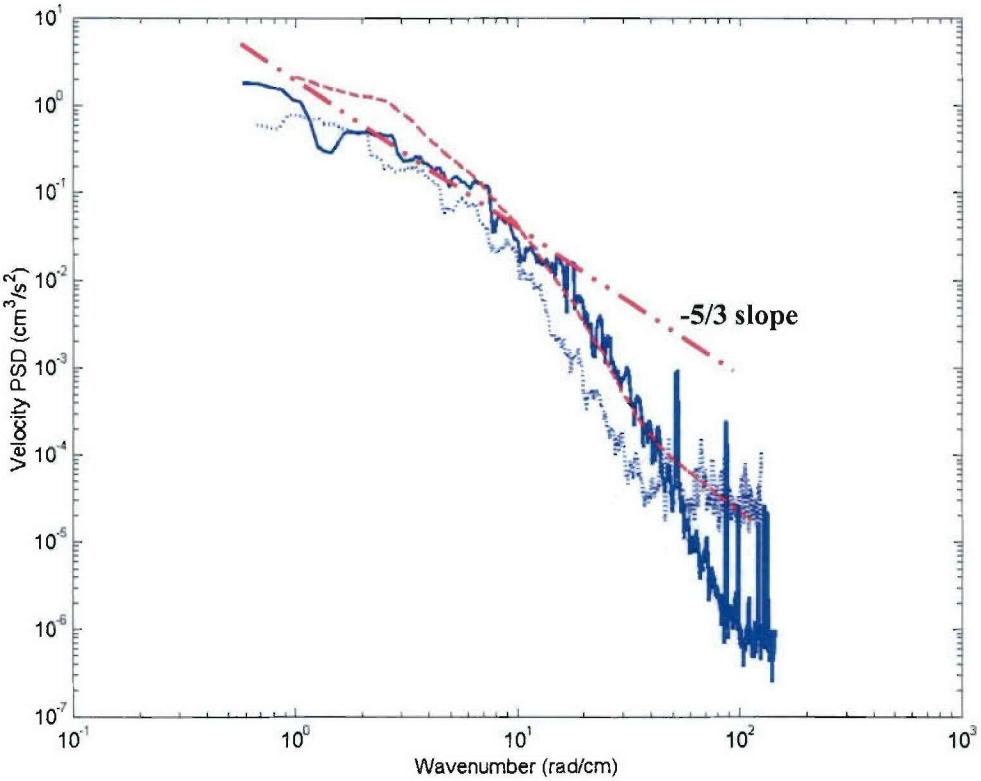

Figure 23. Comparison of spectra from laboratory experiments and the numerical model for the u component of grid-generated turbulent velocity. The solid and dotted lines represent the stratified and nonstratified laboratory data, respectively. The dashed line represents the spectra from the numerical model.

3.4. Summary of the Numerical Simulations

Grid-generated turbulent velocities computed from numerical model simulations were compared with laboratory measurements. The energy levels of the model results are similar to those measured in the laboratory. The model v and w spectra have a –5/3 slope, expected in the inertial subrange. This favorable comparison is achieved in the direct simulation of turbulent flow without prescribing an *a priori* model spectrum either in energy level or spectral shape. These comparison results indicate that direct numerical

simulation of grid-generated turbulence is possible, and that a numerical model can be used for studying the physics of the downstream flow, including shear effects.

The model u spectrum shows unexpected energy due to energetic low wavenumber features. It is hypothesized that these features are eddies that have not yet fully developed into turbulence.

References

Crow, S.C., 1970. Stability theory for a pair of trailing vortices, *AIAA J., 8*, 2172-2179.

Finnigan, T. D., K. B. Winters and G. N. Ivey, 2001. Response characteristics of a buoyancy-driven sea, *J. Phys. Oceanogr., 31*, 2721-2736.

Lai, D. Y. and D. P. Delisi, 2005. Analysis of at-sea turbulent velocity data and spectra, NorthWest Research Associates, Report NWRA-BeCR-05-R304, Bellevue, WA.

Liu, H.T., 1995. Energetics of grid turbulence in a steady stratified fluid, *J. Fluid Mech., 296*, 127-157.

Proctor, F.H., 1987. "The Terminal Area Simulation System, Volume I: Theoretical formulation," NASA Contractor Report 4046, DOT/FAA/PM-86/50, April.

Winters, K. B. and H. E. Seim, 2000. The role of dissipation and mixing in exchange flow through a contracting channel, *J. Fluid Mech., 407, 265-290.*

Winters, K. B., H. E. Seim, and T. D. Finnigan, 2000. Simulation of non-hydrostatic, density-stratified flow in irregular domains, *International Journal of Numerical Methods in Fluids, 32, 263-284.*